



HAL
open science

Synthesis of Redox-Active Photochromic Phenanthrene Derivatives

Elarbi Chatir, Martial Boggio-Pasqua, Frédérique Loiseau, Christian Philouze,
Guy Royal, Saioa Cobo

► **To cite this version:**

Elarbi Chatir, Martial Boggio-Pasqua, Frédérique Loiseau, Christian Philouze, Guy Royal, et al..
Synthesis of Redox-Active Photochromic Phenanthrene Derivatives. *Chemistry - A European Journal*,
2022, 28 (7), pp.e202103755. 10.1002/chem.202103755 . hal-03586676

HAL Id: hal-03586676

<https://hal.science/hal-03586676>

Submitted on 13 Apr 2022

HAL is a multi-disciplinary open access archive for the deposit and dissemination of scientific research documents, whether they are published or not. The documents may come from teaching and research institutions in France or abroad, or from public or private research centers.

L'archive ouverte pluridisciplinaire **HAL**, est destinée au dépôt et à la diffusion de documents scientifiques de niveau recherche, publiés ou non, émanant des établissements d'enseignement et de recherche français ou étrangers, des laboratoires publics ou privés.

Synthesis of Redox-Active Photochromic Phenanthrene Derivatives

Elarbi Chatir^[a], Martial Boggio-Pasqua^[b], Frederique Loiseau^[a], Christian Philouze^[a], Guy Royal^[a], Saioa Cobo *^{[a], [c]}

[a] E.C, Pr. F. L, Dr. C.P, Pr. G. R, Dr. S. C
Univ. Grenoble Alpes, CNRS, DCM,
38000 Grenoble, France
E-mail: Saioa.cobo@univ-grenoble-alpes.fr

[b] Dr. M.B-P
LCPQ UMR 5626, CNRS et Université Toulouse III – Paul Sabatier
118 route de Narbonne,
31062 Toulouse, France

[c] Dr. S. C
Institut Universitaire de France,
1 rue Descartes, 75231 Paris,
France

Supporting information for this article is given via a link at the end of the document.

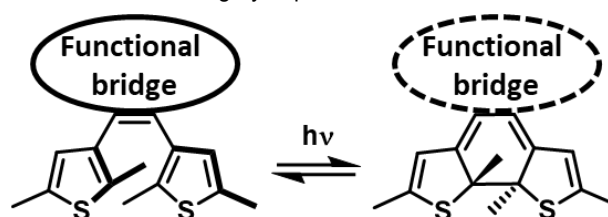
Abstract: A phenanthrene unit has been functionalized by several methylthiophene units in order to bring it a photochromic behavior. These compounds were characterized by NMR, absorption and emission spectroscopies, theoretical calculations as well as cyclic voltammetry. The association of a phenanthrene group with a photochromic center could open the door to a new generation of organic field-effect transistors.

Introduction

Polycyclic aromatic hydrocarbons (PAHs) have focused large interest in the last decade because of their extensive applications in optoelectronic devices, as opto-transistors or in organic field-effect transistors.^[1–3] Since several years the diversifying of the PAH structures with the introduction of hetero-elements has emerged as a priority for the modulation of the electronic properties. This strategy has been notably applied with the introduction of sulfur element through thienyl unit.^[4–9] Indeed, the latest is known to show unique electronic, optical and redox properties.^[10] Moreover, the polarizability of S atoms leads to a stabilization of the conjugated molecules and to excellent charge transport properties, essential for applications in molecular electronics.^[5]

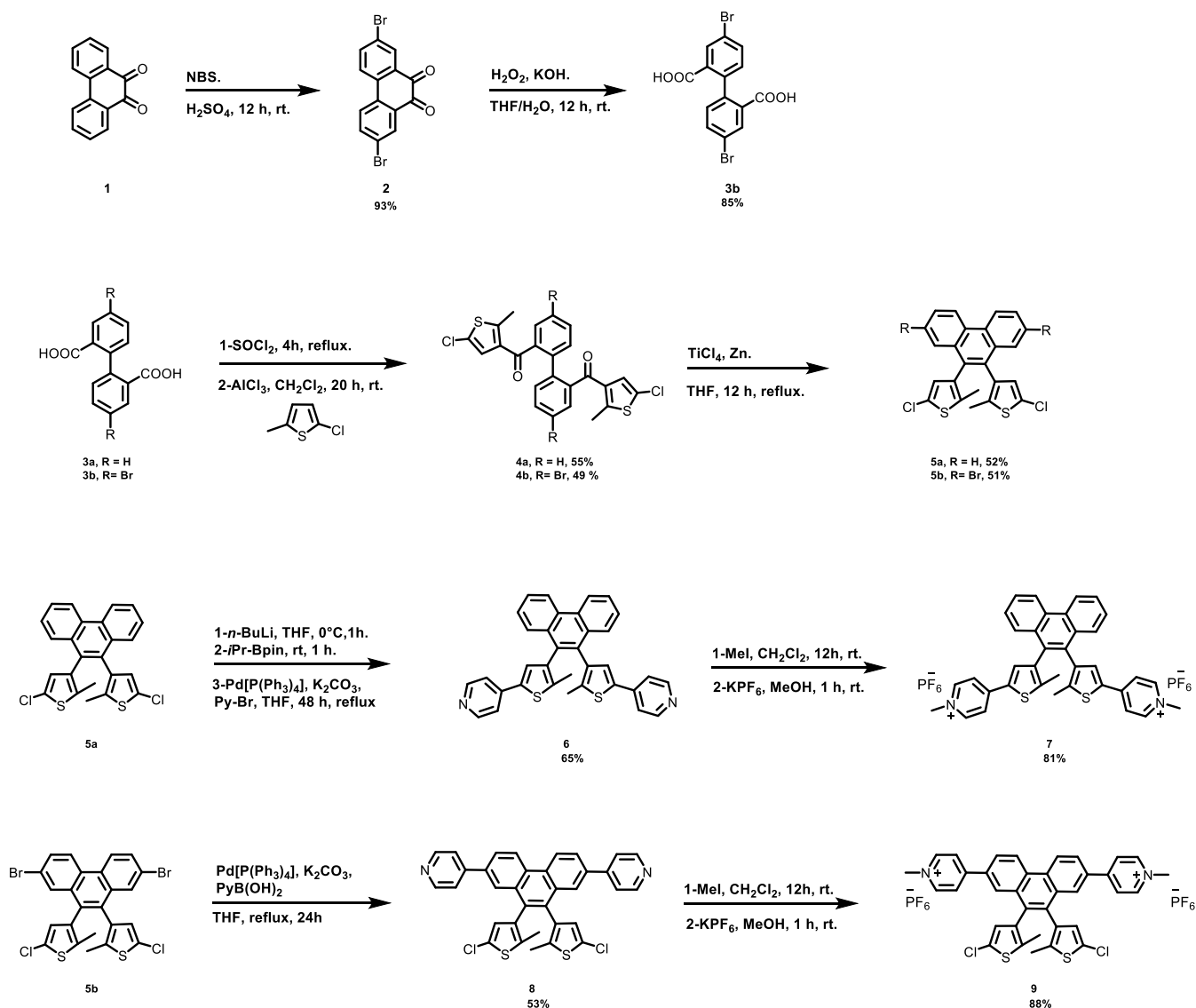
Furthermore, thienyl units are the main constituents in the skeleton of the dithienylethene (DTE) photochromic molecules. DTE is a non-linear compound containing two thiophene groups connected by an ethene bridge. This molecule undergoes a photochemically and electrochemically reversible 6π -electrocyclization between two isomers, namely a low conjugated open form and a high conjugated closed form (Scheme 1).^[11] Several studies have been devoted to the modification of the simple ethene bridge,^[12–15] the most popular and successful being the perfluorocyclopentene derivatives.^[11,16,17] Over the last decade, significant efforts have been made towards the introduction of new aromatic bridges based on PAH instead of the

ethene bridge in the skeleton of DTE molecules. However, to date, only molecules involving phenanthroline and phenanthrene can be included in the category of photochromic PAH.



Scheme 1. Schematic representation of the photochemical isomerization of a dithienylethene.

Phenanthroline-based photochromic materials have been widely used as an efficient coordinating unit in order to build up complexes exhibiting particular fluorescent^[18] or magnetic properties^[19] depending on the photo-isomer. On the contrary, examples concerning the phenanthrene unit are scarce. Feringa *et al.*^[20] described a photochromic phenanthrene derivative in which, for the first time, the photochemistry of individual atropisomers has been studied. This phenomenon has been possible due to the higher energy barrier of the conformations in the phenanthrene derivatives induced by the restricted rotation of the thienyl groups compared to the cyclopentene derivatives. Later, the modification of the phenanthrene entity with coordinating units such as pyridine opened the door to the coordination chemistry field. Thus, Benedict *et al.*^[21,22] reported the synthesis and photochromic properties of a molecular organic framework. Recently, Ma *et al.*^{[23][23]}, synthesized two rhenium compounds from a photochromic ligand in which the rhenium metal center is linked to the phenanthrene through a coordinating unit. However, to date, all investigations involving a phenanthrene unit in the photochromic skeleton of the compounds have been focused on the study of the photochromic properties neglecting



Scheme 2. Synthetic pathways leading to 6_o, 7_o²⁺, 8_o and 9_o²⁺ (o refers to the open form).

the study and the understanding of the electrochemical properties, that are essential for the application of these compounds in the field of switchable molecular electronics. Thus, in order to go a step further, we focus in this paper on the synthesis, photochemical and electrochemical properties of four PAH-DTE derivatives. These compounds contain phenanthrene units as a PAH platform bearing pyridine or N-methyl pyridinium units which can be appended to the thienyl units (6 and 7²⁺) or to the phenanthrene bridge (8 and 9²⁺). The previously synthesized compound 8 by Ma *et al.*^[23] is also reinvestigated. In addition, theoretical calculations based on density functional theory (DFT) and its time-dependent version (TD-DFT) have been performed on selected compounds in order to rationalize the experimental observations.

Results and Discussion

Synthesis and characterisation

The target photochromes 6_o and 8_o and their corresponding quaternized analogues 7_o²⁺ and 9_o²⁺ were prepared following the synthetic route summarized in scheme 2 (o refers to the open form). The synthesis starts with the Friedel–Crafts acylation of 2-chloro-5-methylthiophene with the diacid chloride of diphenic acid generated *in situ*. The resulting diketone is then cyclized under McMurry coupling conditions to yield the dichloride derivative. At this step, the intermediate is subjected to a lithium-halogen exchange followed by a Suzuki–Miyaura coupling reaction to yield 6_o or directly with the same cross-coupling reaction in the presence of 4-pyridylboronic acid and tetrakis(triphenyl)phosphine palladium (0) to yield 8_o as a yellow solid. The bis-N-methylations are achieved using an excess of methyl iodide, and the crude reaction product was subjected to an anion exchange procedure to afford the targeted pyridinium salts 7_o²⁺ and 9_o²⁺ isolated as a yellow powder. All of the compounds were characterized by mass spectrometry and NMR spectroscopy (see the Experimental Section and the Supporting Information).

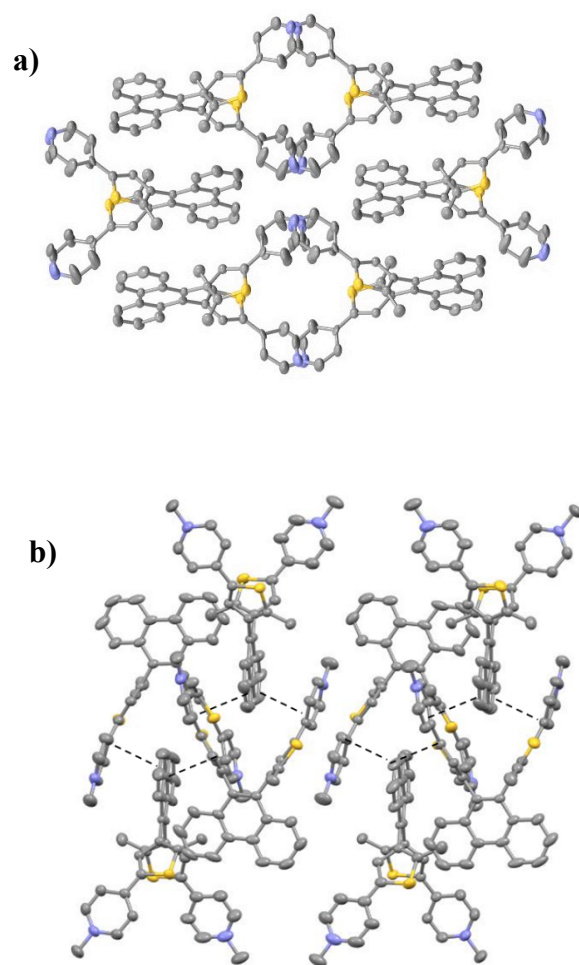


Figure 1. Crystal packing of 6_o (a) and 7_o^{2+} (b) with thermal ellipsoids plotted at the 50% probability level. Hydrogen atoms and PF_6^- anions are omitted for clarity. (Full crystallographic data are provided in ESI)

Compounds 6_o and 8_o crystallize in the monoclinic system $C2/c$ and $P2_1/c$, respectively, with DTE is in its open form. The distances between the two reactive carbon atoms are 4.698 and 4.368 Å for 6_o and 8_o respectively. In both cases the thienyl groups lie in an antiparallel conformation and adopt a perpendicular arrangement with respect to the phenanthrene moiety, with dihedral angles of 90 and 115°, respectively. In the structure 6_o the pyridine units are in nearly coplanar conformation with respect to thiophene in which the dihedral angle of the pyridine rings with respect to the central thiophene ring is 15.1°. In the structure of 8_o the pyridine units exhibit dihedral angles of 32.7° and 49.9° with respect to the phenanthrene group. These two non-cationic structures are stabilized with several intermolecular interactions. 6_o shows a packed structure with two kinds of interactions *i*) a π -stacking morphology with a measured π - π distance of 3.1 Å between the pyridine groups (Figure 1a) and *ii*) Van der Waals interactions between the phenanthrene and the internal methyl of the thienyl counterpart (3.8 Å). These interactions induce a perfect alignment of the phenanthrene bridge which can be seen when looking down the b axis. Contrariwise, on the packing of the

structure 8_o , only Van der Waals interactions can be observed between the pyridine and the phenanthrene units.

The cationic 7_o^{2+} and 9_o^{2+} structures crystallize in $Pcnb$ and $P2_1/c$ orthorhombic system, respectively. Their unit cells show the DTE cation with two PF_6^- counterions. Intermolecularly, 7_o^{2+} possess a 1D-lamellar stacking morphology with a measured π - π distance of 3.3 Å (Figure 1b), suggesting a good molecular orbital contact and the possibility to high mobility charge along this axis.^[24] In contrary, no strong intermolecular interaction has been observed for 9_o^{2+} .

Optical and electrochemical properties

The spectroscopic data found for compounds 6_o , 8_o , 7_o^{2+} and 9_o^{2+} are collected in Table 2. In the 250-800 nm range the absorption spectrum of phenanthrene (10) displays one absorption band at 254 nm attributed to π - π^* transitions. This absorption band is bathochromically shifted by 53 and 32 nm in compounds 6_o (Figure 2) and 8_o (Figure S13b), respectively, in agreement with an extension of the aromatic π -system. The experimental energy gaps are 3.29 and 3.59 eV for 6_o and 8_o , respectively. As expected from the literature data, the bands observed on the spectrum of 6_o and 8_o appear further red shifted in the pyridinium substituted derivatives 7_o^{2+} (Figure S13a) and 9_o^{2+} (Figure 2 and Table 1), thereby, the lowest energy bands for the 7_o^{2+} and 9_o^{2+} compounds are observed around 350-360 nm range (Figures 1 and 2). The experimental energy gaps are 2.97 and 2.89 eV for 7_o^{2+} and 9_o^{2+} , respectively.

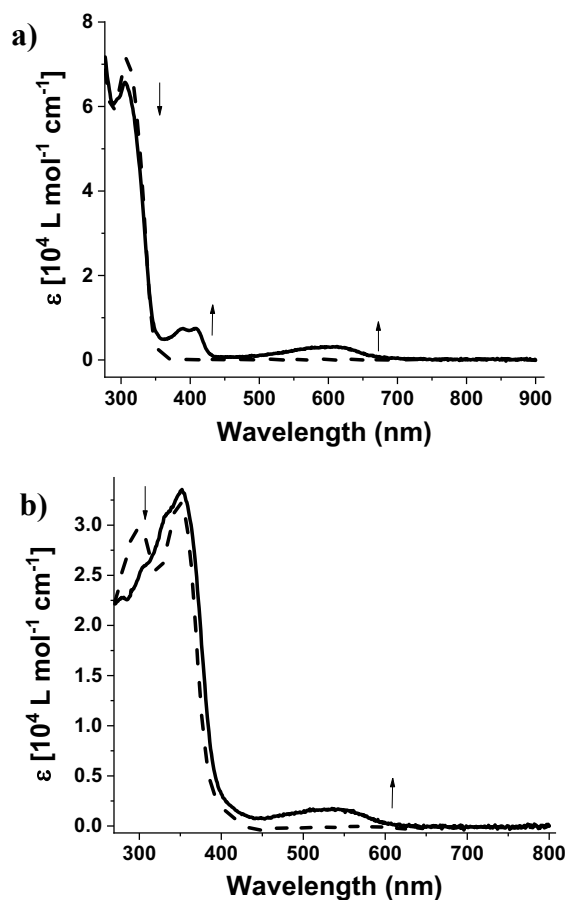


Figure 2. UV-vis spectra evolution before (dashed line) and after (black line) irradiation of 6_o (a) and 9_o^{2+} (b) (CH_3CN , $\lambda = 365$ nm, 14 W).

Table 1: Spectroscopy data.

	λ_{\max} [nm] (ϵ [10^4 L·mol ⁻¹ ·cm ⁻¹])	λ_{em}	ϕ_{em} (λ exc)	τ (ns)	$\phi_{\text{O} \rightarrow \text{C}}$ (365 nm) / $\phi_{\text{O} \rightarrow \text{C}}$ (530 nm)	Energy gap (HOMO/LUMO) (eV)
6_o/6_c	307 (7.1) / 307 (6.5), 389 (0.7), 409 (0.7), 608 (0.2)	397 and 508	0.25 (340)	1.7 and 6.9	[a]	3.29 / 1.74
7_o²⁺/7_c²⁺	365 (5.0) / No isomerisation	572	0.42 (328)	3.1	[a]	2.97
8_o/8_c	287 (8.8) / 263 (4.3), 303 (6.6), 336 (4.5), 555 (0.2)	400	0.30 (340)	1.4	0.015 / 1.2·10 ⁻⁴	3.59 / 1.93
9_o²⁺/9_c²⁺	350 (303) / 345 (305), 550 (0.2)	559	0.23 (313)	2.6	0.031 / 4.6·10 ⁻³	2.89 / 1.99
7_o²⁺/7_c	365 (5.0) / 381 (3.16), 567 (3.43)					2.97 / 1.71
9_o²⁺/9_c	350 (3.3) / 673 (4.71)					2.89 / 2.05
10	254 (6.9)	364	0.13 (293)			

[a] not measurable

The closing process converts a set of two virtually isolated thiophene subunits into a 6 π -electron aromatic system. This process can be easily monitored by UV-vis absorption spectroscopy following the changes occurring in the spectra when samples are submitted to UV irradiation (365 nm). Irradiation of compounds 6_o, 8_o and 9_o²⁺ in acetonitrile leads to a fast (~ 60 s) and moderate decrease of the main absorption band located in the UV region and attributed to the open isomers at the expense of new bands growing in the visible region around 550-600 nm attributed to the closed forms. These results stand in sharp contrast with those obtained under the same conditions with 7_o²⁺ for which no UV-vis spectroscopic changes have been detected even after prolonged irradiation. Nevertheless, a ns-flash photolysis experiment shows the formation of an absorption band in the visible region of the transient absorption spectrum of 7_o²⁺, with a maximum centered at 600 nm (Figure S1). This wavelength corresponds to the domain expected for the absorption of the closed form of compound 7. The absorption band decays back to the ground state in 1025 ns (Figure S2), and is therefore attributed to the re-opening process of the unstable form 7_c.

The kinetic of the back-conversion for the closed isomers 6_c, 8_c and 9_c²⁺ was investigated since the closed forms are not thermally stable. The latter was assessed upon monitoring the changes appearing in the UV-Vis spectra over time at three different temperatures. The rate constants, half-life times and activation energies were calculated assuming a first-order thermal relaxation process. The calculated activation energies are 12 kcal/mol for 6_c, and 18 and 19 kcal/mol for 8_c and 9_c²⁺, respectively, indicating a very low thermal stability for 6_c (the half-life times are less than 1 min at 297 K). These activation energies are consistent with the potential energy barriers computed at the DFT level: 10.9, 15.5 and 15.3 kcal/mol for 6_c, 8_c and 9_c²⁺, respectively (Figures S3-S5). Including thermal and entropic corrections, the activation energies are computed at 8.3, 12.3 and 14.4 kcal/mol respectively.

Emission spectra and excited-state lifetimes in acetonitrile solution for the open compounds have been recorded under inert atmosphere at room temperature. All the spectroscopic data related to emission properties are reported in Table 1. Compound 6_o exhibits two maxima of emission, centered at 397 and 508 nm. The higher energy band of emission brings up a vibronic structure

and is attributed to the radiative deactivation of a π - π^* excited state, essentially centered on the phenanthrene moiety. The second part of the emission profile is likely due to a π -stacking phenomenon between the extended flat surfaces of the phenanthrenes. Indeed, the decay of the emission is biexponential, with a short component of 1.7 ns predominant at high energy, and a longer component of 6.9 ns prevalent in the 500 nm region. Moreover, a 10-fold dilution allows to decrease the ratio of this low-energy emission band (Figure 3). The TD-DFT calculation of the vertical fluorescence transition energy for 6_o predicts an emission wavelength of 379 nm in good agreement with the experimental observation. It also confirms that the emission is due to a π - π^* locally excited state centered on the phenanthrene moiety (Figure S6a). The absence of electronic transition in the 500 nm region corroborates the fact that this emission feature in the visible range is due to aggregation.

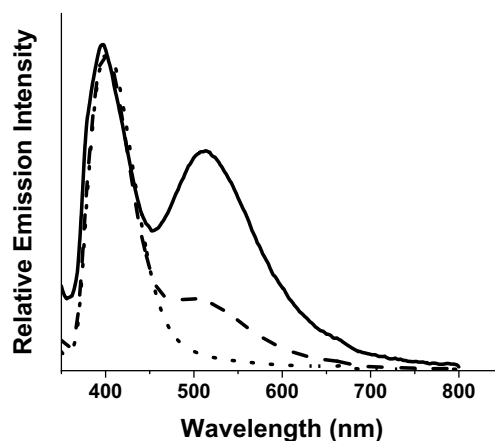


Figure 3. Emission spectra of 6_o at 2·10⁻⁷ M (full line), 6·10⁻⁸ M (dashed line) and 2·10⁻⁸ M (dotted line) in degassed CH₃CN.

The corresponding compound bearing 2 pyridine units on the phenanthrene platform, 8_o, has no possibility of stacking because of the torsion angle between the planes of the phenanthrene and of the pyridine rings. This results in a monoexponential decay of the π - π^* emission with a lifetime of 1.4 ns, centered at 400 nm, red shifted with respect to the one of 6_o because of the presence of the additional rings.

In the case of the quaternized analogues 7_o^{2+} and 9_o^{2+} the shape and energy of emission radically change (see Figure S14). The maxima of emission are red-shifted to 572 and 559 nm respectively, thus displaying substantial Stokes shifts of about 200 nm. In addition, the emission spectra lose their structures and become much wider. This evidences a modification of the nature of the emissive excited state, explained by the presence of the positively-charged pyridiniums that act as strong electron withdrawing subunits and induces the formation of charge transfer excited states. This is further confirmed by the variation of the maximum wavelength of emission as a function of the solvent polarity (Figure S14). The solvatochromism is a characteristic illustrative of a highly dipolar emissive state, such as a charge transfer excited state. Using our TD-DFT protocol, the vertical fluorescence transition energy for 7_o^{2+} is computed at 2.173 eV, corresponding to an emission wavelength of 571 nm, which is in excellent agreement with the experimental observation. The nature of the emissive S_1 state is of clear charge transfer character between the phenanthrene moiety playing the role of the electron donor and the pyridinium groups playing the role of the electron acceptor (Figure S6b).

The electrochemical properties of these derivatives were studied by cyclic voltammetry under an inert atmosphere in acetonitrile containing tetra-*n*-butylammonium perchlorate (TBAP, 0.1 M) as supporting electrolyte. A vitreous carbon disk was used as working electrode. The number of electrons involved in each oxidation or reduction wave were determined by coulometry measurements. The cyclic voltammetry (CV) curves obtained for 7_o^{2+} and 9_o^{2+} isomers are shown in Figures 4 and 5, compounds 6_o and 8_o are not redox actives in the +1/-2V range.

The CV curve of 7_o^{2+} (Figure 4) features a bielectronic irreversible wave at $E_{pc} = -1.42$ V (the intensity of this signal was compared to the wave obtained in the presence of an equimolar solution of ferrocene as internal standard). During the back scan, two anodic irreversible peaks can be observed at much less negative potential at $E_{pa} = -0.73$ and -0.68 V. In agreement with prior studies^[25] and on the basis of DFT calculations, these anodic signals are attributed to the oxidation of a substantial amount of the closed isomer (7_c) generated in situ at the electrode interface during the forward scan down to -1.5 V. Surprisingly, the observed new redox waves are not reversible as observed when reducing the solution, indicating a chemical and thermal instability of the generated 7_c^{2+} which immediately generates the open 7_o^{2+} isomer.

Further insights into the redox behavior of the $7_o^{2+}/7_c$ couple have been provided by spectro-electrochemical measurements. In situ absorption spectra were recorded over time during the potentiostatic reduction of 7_o^{2+} (0.1 mM in CH_3CN) carried out at $E_{app} = -1.5$ V. Selected UV-vis absorption spectra collected throughout the electrolysis are displayed in Figure 4. These data reveal that the reduction with two electrons leads to the formation of a blue solution characterized by an intense absorption band in the visible region at 567 nm associated to an extension of the conjugation of the compound and attributed to the neutral closed form. The reversibility of the redox processes was checked by re-oxidation of the mixture upon setting the potential at -0.65 V. The progressive decrease in intensity of the band at 567 nm, attributed to 7_c , for the benefit of the band attributed to the dicationic open form 7_o^{2+} , at 365 nm is observed. Thus, we can conclude that the

7_c^{2+} is highly unstable and not observable in the experiment conditions. This electrochemical behavior is corroborated by our DFT results. Upon 2 electron-reduction, 7_o^{2+} is expected to undergo a ring-closure to form 7_c , this species being 10 kcal/mol lower than the biradical species 7_o (Figure S7).

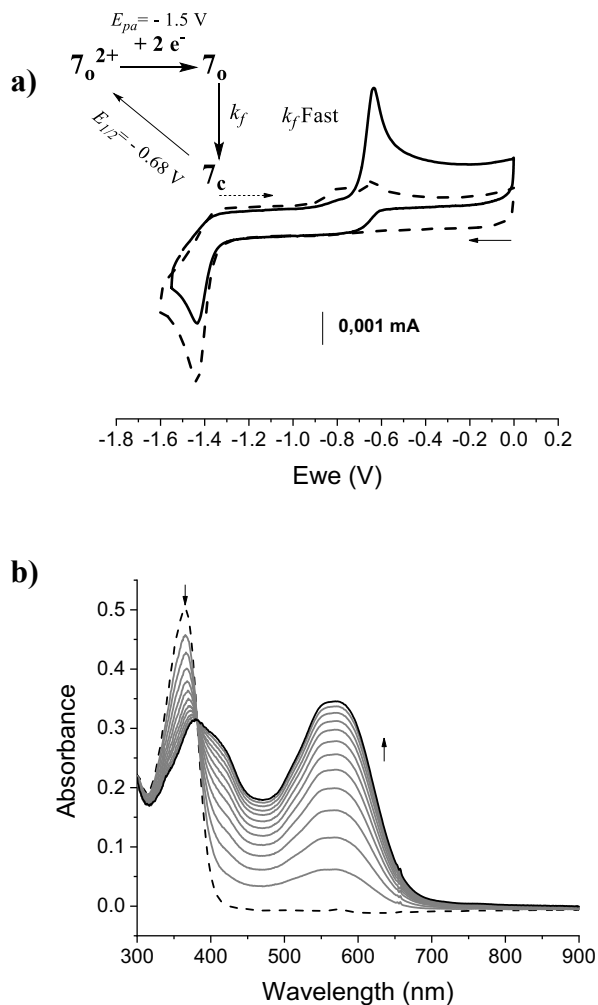


Figure 4. (a) CV curves recorded for 7_o^{2+} before (grey line) and after (black line) electrolysis at -1.5 V. (b) Evolution of the UV-vis absorption spectra during the electrolysis of 7_o^{2+} at $E_{app} = -1.5$ V (initial state, 7_o^{2+} , dashed line) ($[C] = 0.1$ mM in 0.1 M TBAP/ CH_3CN , $v: 100$ mV \cdot s $^{-1}$, VC, $\varnothing = 3$ mm, E (V) vs. Ag^+/Ag 10^{-2} M).

The change of spectral features going from 7_o^{2+} to 7_c is also in line with the experimental observations (Figure S8): emergence of an intense absorption band around 600 nm and decrease of the intensity of the band around 400 nm associated with a blue-shift and a broadening of this band. Note that the instability of the 7_c^{2+} is confirmed by our DFT calculations, as the thermal energy barrier to ring-open is computed at only 7.5 kcal/mol (Figure S9). This low ring-opening energy barrier explains why 7_c^{2+} is not observed upon irradiation of 7_o^{2+} .

From the electrochemistry measurements and UV-vis spectroscopy the energy gap as well as the HOMO (the highest occupied molecular orbital) and LUMO (lowest unoccupied molecular orbital) energy levels of 7_o^{2+} and 7_c have been

calculated. The energy gap is of 2.97 (417 nm) and 1.71 (726 nm) eV and the HOMO/LUMO values are $-6.352/-3.382$ eV and $-3.982/-2.272$ eV for 7_o^{2+} and 7_c respectively. These results are supported by DFT calculations which provide the following HOMO/LUMO energies $-6.149/-2.932$ eV and $-3.950/-1.631$ eV for 7_o^{2+} and 7_c respectively.

The electrochemical behavior of 9_o^{2+} was also studied by cyclic voltammetry (Figure 5). The CV curve of 9_o^{2+} features a reversible bielectronic wave at -1.32 V attributed to the pyridinium moieties. Contrariwise to the electrochemical behaviour of 7_o^{2+} , no wave has been detected during the return scan suggesting that the ring-closure of 9_o^{2+} cannot be achieved through a redox stimulus. In order to investigate the electrochromic properties of the 9_o^{2+} compound in depth, spectro-electrochemical measurements were carried out. The absorption spectra were recorded during the potentiostatic reduction of 9_o^{2+} (0.1 mM in CH_3CN) performed at -1.5 V. Selected UV-vis absorption spectra collected throughout the electrolysis are displayed in Figure 5.

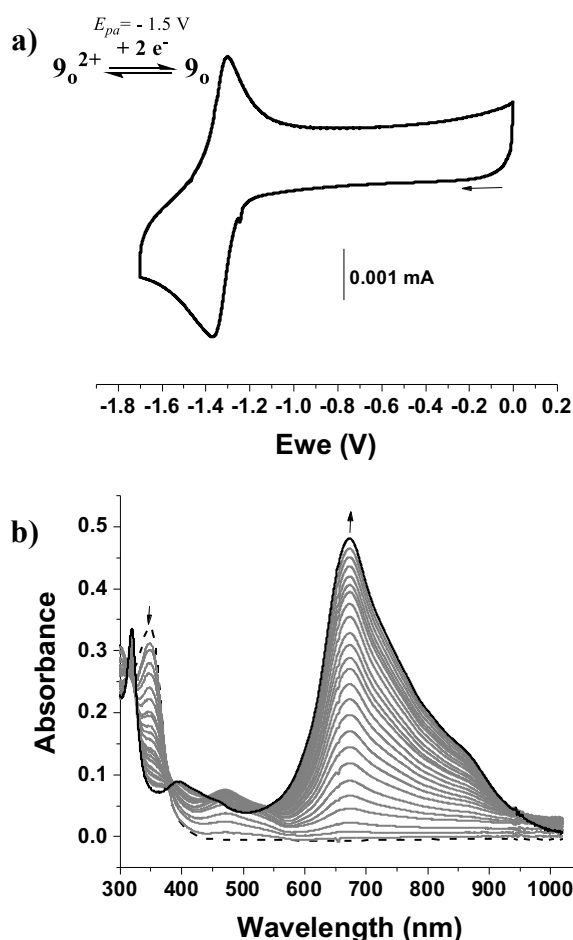
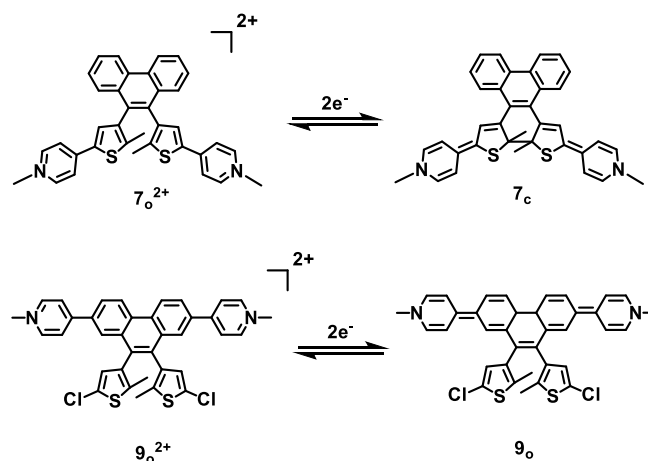


Figure 5. (a) CV curves recorded for 9_o^{2+} . (b) Evolution of the UV-vis absorption spectra during the electrolysis of 9_o^{2+} at $E_{\text{app}} = -1.5$ V (initial state, 9_o^{2+} , dashed gray) ($[C] = 0.1$ mM in 0.1 M TBAP/ CH_3CN , ν : $100 \text{ mV}\cdot\text{s}^{-1}$, VC, $\varnothing = 3$ mm, E (V) vs. Ag^+/Ag 10^{-2} M).

Starting from a light-yellow solution characterized by a single absorption band at 348 nm in the UV region, the solution becomes

dark blue, the UV band disappear and new bands emerge in the visible region (474 and 673 nm). This spectro-electrochemical experiment results combined with the absence of a redox wave on the return scan during the cyclic voltammetry of 9_o^{2+} suggest that the intense blue color of the solution is due to the reduction of pyridinium units on the 9_o^{2+} form to afford 9_o . Thus, it can be concluded that the closed isomer cannot be formed when the pyridinium units are in the 2 and 7 positions of the phenanthrene. In order to confirm the formation of the 9_o compound the spectro-electrochemical properties of a reference compound in which the phenanthrene bridged two pyridinium units (15 see figure S15) has been investigated. The CV of the reference compound presents a reversible redox wave located at -1.34 V. During the electrochemical reduction at $E_{\text{app}} = -1.5$ V, the solution goes from yellow to blue, and the maximum of the absorption spectra shifts from 350 to 658 nm. Indicating that the color change can also be induced by the electrochemical reduction of the pyridinium units. These observations are supported by our DFT calculations. Upon 2 electron-reduction, 9_o^{2+} is predicted to form 9_o without formation of the closed form 9_c (Scheme 3). Indeed, 9_c is located 27 kcal/mol above 9_o and involves a potential energy barrier for the thermal ring-closing reaction over 40 kcal/mol (Figure S10). The change of spectral features going from 9_o^{2+} to 9_o (Figure 11) is also in line with the experimental observations (Figure 5): appearance of an absorption band around 700 nm. This band in the red region for 9_o is due to the increased conjugation between the pyridinium units and the phenanthrene moiety that become nearly coplanar (Figures S5 and S10). This change of spectral feature is thus only attributed to the reduction of the pyridinium units, which is confirmed by the absorption spectra of the bispyridinium phenanthrene system (15) showing the same spectral changes from the dicationic to the reduced neutral species (Figure S12 can be compared with Figure S15).



Scheme 3. Summary of the electrochemical behavior of 7_o^{2+} and 9_o^{2+} .

Conclusion

In conclusion, the different pattern for the substitution of compound 6_o and 8_o as well as for 7_o^{2+} and 9_o^{2+} yields to a drastic difference of photo- and electrochemical behavior. 6_o and 8_o , compounds bearing pyridine units present a similar photochromic behavior. However, the thermal stability of the closed form is

much longer for the compound **8_c** (more than 30 times) in which the pyridines are diametrically in the opposite positions of the phenanthrene. **7_o²⁺** and **9_o²⁺** are electrochemically active compounds. The reduced form of compound **7_o²⁺** leads to the reduced closed form, **7_c**, whereas the reduction of compound **9_o²⁺** inevitably yields to the reduced open form, **9_o** (Scheme 3). It appears that only the adjacent electron-withdrawing substituents can display a redox closing process. The reduction of substituents at diametrically opposite positions of the phenanthrene are totally independent from the photochromic counterpart as demonstrated by the spectro-electrochemistry experiments and DFT/TD-DFT calculations. Moreover, some of these compounds, notably **6_o** and **7_o²⁺** show strong intermolecular interactions, *i.e.* good molecular orbital contact, suggesting a high mobility charge. This strategy, utilizing PAH as bridge can be then widely used for the control of switching processes in DTE derivatives, in order to attempt efficient compounds for applications in molecular electronics.

Acknowledgements

This work was granted access to the HPC resources of CALMIP supercomputing center under the allocation 2021-[12158].

Experimental Section

All solvents were purchased and used as received except THF that was distilled over sodium/ benzophenone under argon. Water was purified by reverse osmometry with an Elgastat purification system (5 MΩ.cm). Organic and inorganic reagents used in the procedures described below were purchased on Aldrich, Acros, Fluorochem or TCI Europe and used without further purification. All evaporations were carried out under reduced pressure with a rotatory evaporator, and all organic extract were washed with water and dried with MgSO₄. Silica gel (SiGel), used for column chromatography, refers to Merck silica gel, 40-63 μm. ¹H NMR and ¹³C NMR spectra were recorded on a Bruker Avanced 500 or 400 MHz spectrometer. Chemicals shifts are calibrated to residual solvent peaks. Coupling constant values (J) are given in hertz and chemical shifts (δ) in ppm. High-resolution mass spectrometry analyses were conducted using the HRMS, Bruker maXis mass spectrometer and were performed in positive Electrospray Ionisation (ESI+) at the DCM mass facility. Data for single crystal X-Ray diffraction were collected at 200 K on a Bruker AXS Enraf-Nonius Kappa APEXII diffractometer using the Mo-Kα monochromated radiation. Intensity data were corrected for Lorentz and polarization effects with EVAL 14 and for absorption using SADABS. Structures solutions and refinements were performed with the SHELX softwares implemented by Olex2. All non-hydrogen were refined by full matrix least-squares with anisotropic thermal parameters. Hydrogen atoms were introduced at calculated positions as riding atoms. Crystallographic structures were drawn with the Mercury 2020.3.0 software. A summary of the data collection and structure refinements is provided in the supplementary information. CCDC 2114398-402 contains the supplementary crystallographic data for this paper (Table S1). These data can be obtained free of charge from The Cambridge Crystallographic Data Centre via www.ccdc.cam.ac.uk/data_request/cif. Deposition Number(s) <https://www.ccdc.cam.ac.uk/services/structures?id=doi:10.1002/chem.202103755> (for 5a), 2114399 (for 5b), 2114401 (for 6),

2114402 (for 7), 2114400 (for 9) contain(s) the supplementary crystallographic data for this paper. These data are provided free of charge by the joint Cambridge Crystallographic Data Centre and Fachinformationszentrum Karlsruhe <http://www.ccdc.cam.ac.uk/structures> Access Structures service.

Electrochemical measurements (cyclic voltammetry, CV) were conducted under an argon atmosphere with a standard one-compartment, three-electrode electrochemical cell using a Bio-logic SP300 potentiostat. Anhydrous CH₃CN was used as solvents and tetra-*n*-butylammonium hexafluorophosphate (TBAPF₆, 0.1M) was used as supporting electrolyte. CH-Instrument vitreous carbon (3 mm in diameter) working electrodes were used for CV experiments. Electrodes were polished with 1 μm diamond paste (Mecaprex Presi) prior to each recording. Counter-electrode was a platinum wire immersed directly in the solution. A CH-Instrument AgNO₃/Ag (10⁻² M + tetra-*n*-butylammonium perchlorate 10⁻¹ M in CH₃CN) electrode was used as a reference electrode and the potential of the regular ferrocenium / ferrocene (Fc⁺/Fc) redox couple in acetonitrile is 0.07 V under our experimental conditions. Cyclic voltammetry (CV) curves were recorded at a scan rate of 0.1 V s⁻¹. An automatic ohmic drop compensation procedure was systematically implemented prior to recording CV data. UV-vis spectroelectrochemical experiments were carried out with a photodiode array UV-vis NIR spectrometer MCS 501 UV-NIR (Carl Zeiss). The light sources were halogen CLH 500 (20 W) and deuterium CLD 500 lamps with an optical fiber 041.002-UV SN 012105 or using an additional 1 mm quartz immersion probe (Hellma) and an automatic shutter. UV- light irradiations have been performed at 366 nm using a hand UV-lamp. Synthetic procedures. 2,7-dibromophenanthrene-9,10-dione, 4,4'-dibromo-[1,1'-biphenyl]-2,2'-dicarboxylic acid, 2-chloro-5-methylthiophene, [1,1'-biphenyl]-2,2'-diylbis((5-chloro-2-methylthiophen-3-yl)methanone), (4,4'-dibromo-[1,1'-biphenyl]-2,2'-diyl)bis((5-chloro-2-methylthiophen-3-yl)methanone), 9,10-bis(5-chloro-2-methylthiophen-3-yl)phenanthrene and 3,3'-(2,7-dibromophenanthrene-9,10-diyl)bis(5-chloro-2-methylthiophene) were synthesized following reported procedure (see SI).

9,10-bis(2-methyl-5-(pyridin-4-yl)thiophen-3-yl)phenanthrene (6_o): Under argon atmosphere, 9,10-bis(5-chloro-2-methylthiophen-3-yl)phenanthrene (500 mg, 1.13 mmol, 1 eq.) was dissolved in a dry THF (10 ml). 2.5 M *n*-BuLi hexane solution (0.92 ml, 2.48 mmol, 2.05 eq.) was added dropwise to the solution at 0°C. The reaction mixture was allowed to warm to r.t. and stirred for 1 h. Then 2-Isopropoxy-4,4,5,5-tetramethyl-1,3,2-dioxaborolane (0.56 ml, 2.54 mmol, 2.24 eq.) was added and the reaction was stirred during 1 h at r.t. Degassed aq. 3 M Na₂CO₃ (2.26 mL, 6.78 mmol, 6 eq.), Pd(PPh₃)₄ (59 mg, 0.056 mmol, 5% mmol) and the 4-bromopyridine (446.35 mg, 2.82 mmol, 2.5 eq.) were added and the mixture was heated at reflux for 12 h. The crude was then extracted with Et₂O (3 x 50 ml), dried over Na₂SO₄ and the solvents were evaporated. Purification by chromatography on silica gel using the AcOEt/MeOH (100% to 9 : 1) afford 380 mg (65%) of the product (**6_o**) as a yellow solid. ¹H NMR (500 MHz, CDCl₃-d) δ: 8.84 (d, J = 8.3 Hz, 2H), 8.53 (d, J = 6.3 Hz, 4H), 7.75 – 7.70 (m, 2H), 7.67 – 7.61 (m, 2H), 7.61 – 7.56 (m, 2H), 7.32 (d, J = 6.3 Hz, 4H), 7.19 (s, 2H), 2.20 (s, 6H). ¹³C NMR (125 MHz, Chloroform-d) δ: 150.27, 141.59, 138.82, 137.90, 136.93, 132.71, 131.37, 130.50, 127.73, 127.33, 127.22, 127.11, 122.99, 119.45, 14.73. HRMS (ESI) m/z: Calc. for C₃₄H₂₅S₂⁺ 525.14537. Found. 525.14362.

4,4'-(phenanthrene-9,10-diyl)bis(5-methylthiophene-4,2-diyl)bis(1-methylpyridin-1-ium) hexafluorophosphate (7_o²⁺): To a solution of (**6_o**) (30, mg, 0.057 mmol) in dry DCM (3 ml) was added methyl iodide (1 mL,

large excess). The reaction was stirred at room temperature for 24 h. The resulting suspension was filtered. The solid was collected upon filtration and dissolved in a minimum amount of hot CH₃OH. Upon the dropwise addition of an aqueous concentrated KPF₆ solution. The product precipitated as a yellow powder. It was then collected by filtration, washed with water, and dried under vacuum to give 39 mg (81%) of the product (**7_o²⁺**) as a yellow solid. ¹H NMR (500 MHz, Acetonitrile-*d*₃) δ: 8.96 (d, *J* = 8.3 Hz, 2H), 8.38 (d, *J* = 7.2 Hz, 4H), 7.91 (d, *J* = 7.1 Hz, 4H), 7.81 (ddd, *J* = 8.3, 6.9, 1.4 Hz, 2H), 7.74 (s, 2H), 7.65 (ddd, *J* = 8.1, 6.9, 1.1 Hz, 2H), 7.56 (dd, *J* = 8.3, 1.3 Hz, 2H), 4.16 (s, 6H), 2.28 (s, 6H). ¹³C NMR (125 MHz, Acetonitrile-*d*₃) δ: 149.40, 147.59, 146.02, 140.51, 134.61, 134.26, 132.88, 131.76, 131.41, 128.73, 128.68, 127.67, 124.28, 122.65, 27.62, 15.29. HRMS (ESI) *m/z*: Calc. for [M+2H]²⁺ C₃₆H₃₀N₂S₂ 277.09197. Found. 277.092001.

4,4'-(9,10-bis(5-chloro-2-methylthiophen-3-yl)phenanthrene-2,7-diyl)dipyridine (8_o): In a 100 mL Schlenk tube 3,3'-(2,7-dibromophenanthrene-9,10-diyl)bis(5-chloro-2-methylthiophene) (80 mg, 0.13 mmol, 1 eq.), 4-pyridyl boronic acid (36.2 mg, 0.29 mmol, 2.2 eq.), Na₂CO₃ (81.9 mg, 0.78 mmol, 6 eq.) and Pd(PPh₃)₄ (9 mg, 0.0065 mmol) were added under argon flow to a degassed mixture of water (1 mL) and toluene (8 mL). The solution was then heated under argon at 100 °C for 24 hours. The reaction was cooled to room temperature, the aqueous phase was then extracted with DCM (2x15 mL). The organic phase was washed with water (10 mL), sat. brine solution (10 mL). The organic phase was dried over Mg₂SO₄, and then purified by column chromatography (AcOEt/MeOH 1:0 to 9:1) to give the product (**8**) as a yellow solid (42 mg, 53%). ¹H NMR (500 MHz, Chloroform-*d*) δ: 8.92 (d, *J* = 8.7 Hz, 2H), 8.71 (d, *J* = 6.3 Hz, 4H), 8.03 – 7.99 (m, 2H), 7.91 (d, *J* = 2.0 Hz, 1H), 7.87 (d, *J* = 2.0 Hz, 1H), 7.61 – 7.42 (m, 4H), 6.62 (s, 1H), 6.57 (s, 1H), 2.10 (s, 3H), 2.05 (s, 3H). ¹³C NMR (125 MHz, Chloroform-*d*) δ: 150.54, 150.51, 150.45, 147.75, 137.24, 137.19, 135.23, 135.09, 134.75, 134.42, 133.56, 131.99, 130.31, 130.29, 128.89, 127.63, 126.31, 126.27, 125.95, 125.93, 125.53, 125.39, 124.19, 121.94, 121.84, 121.81, 14.35. HRMS (ESI) *m/z*: Calc. for [M+H]⁺ C₃₄H₂₃N₂Cl₂S₂⁺ 593.06742. Found. 593.06609.

4,4'-(9,10-bis(5-chloro-2-methylthiophen-3-yl)phenanthrene-2,7-diyl)bis(1-methylpyridin-1-ium) hexafluorophosphate (9_o²⁺): To a stirred solution of (**4_o**) (30, mg, 0.057 mmol) in dry CHCl₃ (3 mL) was added methyl iodide (1 mL, large excess). The reaction was stirred at 60 °C for 24 h. After cooling, the resulting suspension was filtered. The solid was collected upon filtration and dissolved in a minimum amount of hot CH₃OH. Upon the dropwise addition of an aqueous concentrated KPF₆ solution. The product precipitated as a yellow powder. It was then collected by filtration, washed with water, and dried under vacuum to give 36.8 mg (80%) of the product (**9_o²⁺**) as a yellow solid. ¹H NMR (500 MHz, Acetonitrile-*d*₃) δ: 9.18 (d, *J* = 10 Hz, 2H), 8.65 (d, *J* = 6.4 Hz, 4H), 8.29 – 8.24 (m, 6H), 8.07 (dd, *J* = 10.8, 2.1 Hz, 2H), 6.81 (s, 1H), 6.73 (s, 1H), 4.31 (s, 6H), 2.11 (s, 3H), 2.06 (s, 3H). ¹³C NMR (125 MHz, Acetonitrile-*d*₃) δ: 156.27, 146.27, 137.37, 135.20, 135.07, 134.84, 134.66, 133.25, 133.21, 132.59, 130.23, 128.86, 127.94, 127.81, 126.55, 126.24, 48.53, 14.35. HRMS (ESI) *m/z*: Calc. for [M]²⁺ C₃₆H₂₈N₂Cl₂S₂²⁺ 311.05300 Found. 311.0561.

Computational Section

DFT and TD-DFT calculations were all carried out with the Gaussian16 package^[26] Ground-state geometry optimizations were performed with the B3LYP functional^[27] along with the 6-31G* basis set^[28,29] Vertical absorption transition energies were computed with the PBE0 functional^[30] and the more extended 6-311+G** basis set^[31,32] The versatile MN15

functional^[33] was used for excited-state geometry optimizations and vertical fluorescence transition energy calculations. The solvent effects were accounted for using the integral equation formalism version of the polarizable continuum model (IEFPCM)^[34] All calculations were performed in the acetonitrile (ε=35.688) solvent. Vertical absorption transition energies were computed using linear-response non-equilibrium solvation. Calculations of the emission wavelengths were carried out using the more accurate state-specific non-equilibrium approach of Impropa and coworkers^[35,36] Vibrational harmonic frequency calculations were performed at the optimized geometries to verify the nature of the stationary points (minimum or saddle point) on the potential energy surfaces and to obtain thermal corrections and entropic contributions to compute Gibb's free energies of reaction and activation energies. Open-shell singlet (diradical) species were calculated using broken-symmetry DFT calculations. Spin-projected energies were obtained with an approximate spin-correction procedure to account for the spin contamination.^[37,38] Gibb's free energies for these open-shell singlet species were computed by using the spin-projected energies. All the convoluted absorption spectra were obtained using a phenomenological Gaussian broadening characterized by a half-width at half-height of 1500 cm⁻¹ for each vertical transition. All the Cartesian coordinates and energies are provided in Table S2.

Keywords: Dithienylethene • redox properties • photochromism • phenanthrene • DFT calculations

- [1] H. J. Yun, D. S. Chung, I. Kang, J. W. Park, Y. H. Kim, S. K. Kwon, *J. Mater. Chem.* **2012**, 22, 24924.
- [2] K. Islam, H. Narjinari, A. Kumar, *Asian J. Org. Chem.* **2021**, 10, 1544.
- [3] D. Elkington, N. Cooling, W. Belcher, P. C. Dastoor, X. Zhou, *Electron.* **2014**, 3, 234.
- [4] W. Delaunay, R. Szucs, S. Pascal, A. Mocanu, P. A. Bouit, L. Nyulászi, M. Hissler, *Dalt. Trans.* **2016**, 45, 1896.
- [5] A. Mishra, C. Q. Ma, P. Bäuerle, *Chem. Rev.* **2009**, 109, 1141.
- [6] J. Roncali, *Chem. Rev.* **1997**, 97, 173.
- [7] R. Benshafrut, M. Rabinovitz, R. E. Hoffman, N. Ben-Mergui, K. Müllen, V. S. Iyer, *European J. Org. Chem.* **1999**, 37.
- [8] X. Feng, J. Wu, M. Ai, W. Pisula, L. Zhi, J. P. Rabe, K. Müllen, *Angew. Chemie - Int. Ed.* **2007**, 46, 3033.
- [9] Y. Chen, W. Chen, Y. Qiao, G. Zhou, *Chem. - A Eur. J.* **2019**, 25, 9326.
- [10] C. J. Martin, B. Gil, S. D. Perera, S. M. Draper, *Chem. Commun.* **2011**, 47, 3616.
- [11] M. Irie, T. Fukaminato, K. Matsuda, S. Kobatake, *Chem. Rev.* **2014**, 114, 12174.
- [12] M. Irie, M. Mohri, *J. Chem. Soc. Chem. Commun.* **1988**, 803.
- [13] S. Chen, W. Li, X. Li, W. H. Zhu, *J. Mater. Chem. C* **2017**, 5, 2717.
- [14] M. Kong, X. Feng, J. Li, J. Wang, Y. Q. Zhang, Y. Song, *New J. Chem.* **2020**, 44, 20129.
- [15] N. F. König, D. Mutruc, S. Hecht, *J. Am. Chem. Soc.* **2021**, 143, 9162.
- [16] M. Hanazawa, R. Sumiya, Y. Horikawa, M. Irie, *J. Chem. Soc., Chem. Commun.* **1992**.
- [17] D. Bléger, S. Hecht, *Angew. Chem. Int. Ed.* **2015**, 54, 11338.
- [18] V. W. W. Yam, C. C. Ko, N. Zhu, *J. Am. Chem. Soc.* **2004**, 126, 12734.

- [19] M. Mörtel, A. Witt, F. W. Heinemann, S. Bochmann, J. Bachmann, M. M. Khusniyarov, *Inorg. Chem.* **2017**, *56*, 13174.
- [20] M. Walko, B. L. Feringa, *Chem. Commun.* **2007**, 1745.
- [21] I. M. Walton, J. M. Cox, C. A. Benson, D. G. Patel, Y. S. Chen, J. B. Benedict, *New J. Chem.* **2016**, *40*, 101.
- [22] I. M. Walton, J. M. Cox, J. A. Coppin, C. M. Linderman, D. G. Patel, J. B. Benedict, *Chem. Commun.* **2013**, *49*, 8012.
- [23] G. X. Jin, T. Wang, Y. Sun, Y. L. Li, J. P. Ma, *Inorg. Chem.* **2020**, *59*, 15019.
- [24] M. S. Little, The Synthesis of Novel Polycyclic Aromatic Hydrocarbons: The Search for Organic Semiconductor Materials, The University of Manchester, **2014**.
- [25] A. Peters, N. R. Branda, *Chem. Commun.* **2003**, 954.
- [26] M. J. Frisch, G. W. Trucks, H. B. Schlegel, G. E. Scuseria, M. A. Robb, J. R. Cheeseman, G. Scalmani, V. Barone, G. A. Petersson, H. Nakatsuji, X. Li, M. Caricato, A. V. Marenich, J. Bloino, B. G. Janesko, R. Gomperts, B. Mennucci, H. P. Hratchian, J. V. Ortiz, A. F. Izmaylov, J. L. Sonnenberg, D. Williams-Young, F. Ding, F. Lipparini, F. Egidi, J. Goings, B. Peng, A. Petrone, T. Henderson, D. Ranasinghe, V. G. Zakrzewski, J. Gao, N. Rega, G. Zheng, W. Liang, M. Hada, M. Ehara, K. Toyota, R. Fukuda, J. Hasegawa, M. Ishida, T. Nakajima, Y. Honda, O. Kitao, H. Nakai, T. Vreven, K. Throssell, J. A. Montgomery, Jr., J. E. Peralta, F. Ogliaro, M. J. Bearpark, J. J. Heyd, E. N. Brothers, K. N. Kudin, V. N. Staroverov, T. A. Keith, R. Kobayashi, J. Normand, K. Raghavachari, A. P. Rendell, J. C. Burant, S. S. Iyengar, J. Tomasi, M. Cossi, J. M. Millam, M. Klene, C. Adamo, R. Cammi, J. W. Ochterski, R. L. Martin, K. Morokuma, O. Farkas, J. B. Foresman and D. J. Fox, *Gaussian 16, Rev. B.01*, Gaussian, Inc., Wallingford CT, **2016**.
- [27] A. D. Becke, *J. Chem. Phys.* **1993**, *98*, 5648.
- [28] W. J. Hehre, K. Ditchfield, J. A. Pople, *J. Chem. Phys.* **1972**, *56*, 2257.
- [29] P. C. Hariharan, J. A. Pople, *Theor. Chim. Acta* **1973**, *28*, 213.
- [30] C. Adamo, V. Barone, *J. Chem. Phys.* **1999**, *110*, 6158.
- [31] R. Krishnan, J. S. Binkley, R. Seeger, J. A. Pople, *J. Chem. Phys.* **1980**, *72*, 650.
- [32] T. Clark, J. Chandrasekhar, G. W. Spitznagel, P. V. R. Schleyer, *J. Comput. Chem.* **1983**, *4*, 294.
- [33] H. S. Yu, X. He, S. L. Li, D. G. Truhlar, *Chem. Sci.* **2016**, *7*, 5032.
- [34] J. Tomasi, B. Mennucci, R. Cammi, *Chem. Rev.* **2005**, *105*, 2999.
- [35] R. Improta, V. Barone, G. Scalmani, M. J. Frisch, *J. Chem. Phys.* **2006**, *125*, 054103.
- [36] R. Improta, G. Scalmani, M. J. Frisch, V. Barone, *J. Chem. Phys.* **2007**, *127*, 074504.
- [37] K. Yamaguchi, F. Jensen, A. Dorigo, K. N. Houk, *Chem. Phys. Lett.* **1988**, *149*, 537.
- [38] S. Yamanaka, T. Kawakami, H. Nagao, K. Yamaguchi, *Chem. Phys. Lett.* **1994**, *231*, 25.